Chapter 1
Modal Identification from Dynamic Signals Obtained from OFDR Distributed Fiber Optics

Patrick Brewick

Abstract Among the many sensing technologies utilized for health monitoring, fiber optics are emerging as a popular choice for monitoring non-standard structures such as pipelines, offshore platforms, and marine structures due to their imperviousness to environmental disturbances and flexible sensing arrangements. Further, the current state-of-the-art in fiber optic technologies can embed dense arrays of sensing points along a single, continuous fiber, creating powerful distributed sensing systems. Optical frequency domain reflectometry (OFDR) is one such distributed sensing technique that utilizes weak continuous fiber Bragg gratings (FBGs) to infer strain along the length of the fiber. Recent advances in OFDR interrogation techniques allow for sampling rates fast enough to capture dynamic effects.

This study will present some results obtained from performing experimental modal analysis on a cantilevered plate using an OFDR distributed fiber optic sensing system (FOSS). Two different dynamic quantities of interest are produced by the OFDR FOSS, both the strains and carrier frequencies at each FBG. Modal analysis is performed using the blind source separation method on both sets of dynamic time histories, yielding high quality estimates of modal frequencies and mode shapes. Details on the quality of modal identification with carrier frequencies will be discussed and a comparison against the strain-based results will be presented.

Keywords Distributed fiber optics · modal identification · strain sensing · carrier frequencies · blind source separation

Introduction

Structural health monitoring (SHM) has been utilized across the engineering community to collect data from a variety of systems and structures, spanning civil infrastructure [1], aerospace structures [2] and marine craft [3], among other dynamical systems [4]. Amidst the different sensor technologies commonly deployed for SHM, fiber optic sensing systems (FOSS) have emerged as a powerful tool for conducting SHM via strain sensing [5–7], where FOSS constitute a broad class of sensors that use various optical phenomena, e.g., intensity modulation, scattering, optical loss, and polarization, to respond to strain [8].

The increasing utilization of FOSS for SHM solutions is partly due to its invulnerability to harsh conditions since the fiber is insensitive to electro-magnetic effects, resistant to corrosion, and maintains reliable operability across a wide range of temperatures [9]. The relative flexibility of fiber also allows it to be outfitted in a variety of geometric patterns and designs [10], matching other highly configurable and modular sensing technologies. These desirable qualities have made FOSS a popular choice for marine and aerospace applications, but efforts to monitor civil infrastructure have also benefited from FOSS [5]. One particular challenge that has arisen, however, is that SHM of large civil structures typically operates on vibrations-based monitoring [11], but the dynamic strains induced by operational loading conditions are often quite small, e.g., below one microstrain [12]. In the past, this limited the utilization of even traditional strain sensors for operational (OMA) to only a few studies, e.g., [13, 14].

Recent developments in the optical interrogation and signal processing of fiber-based strain sensors have demonstrated that sufficient sensitivity and accuracy are, in fact, attainable for vibrations-based SHM with FOSS [12]. Further, the high sensitivity of strain-based features to local damage [15] has led strain modes to emerge as an attractive alternative to more conventional displacement-based mode shapes [16]. For instance, utilizing a series of discrete fiber Bragg grating (FBG) sensors, Wang et al. [17] recovered strain mode shapes and modal parameters by fitting polynomials to the strain power

Patrick Brewick
Department of Civil and Environmental Engineering & Earth Sciences
University of Notre Dame, Notre Dame, IN 46561
e-mail: pbrewick@nd.edu

Brandon Dilworth et al. (eds.), *Topics in Modal Analysis & Parameter Identification II, Vol. 10*, Conference Proceedings of the Society for Experimental Mechanics Series, https://doi.org/10.13052/97887-438-0155-9_1

spectral density functions. Anastasopoulos et al. have similarly deployed discrete FBGs to collect strain information and subsequently perform OMA using stochastic subspace identification techniques on a variety of structures, including experimental prestressed concrete beams [12], a steel I-beam [16] and a steel arch bridge [18].

Distributed sensing, such as that offered by more advanced FOSS [19], provides a contrast to traditional SHM that uses discrete sensing points since distributed FOSS yields a high density of sampling points all within a single sensor (fiber). While several techniques have been employed for distributed sensing [20], NASA has developed a distributed FOSS that utilizes optical frequency domain reflectometry (OFDR) technology. OFDR has been shown to reliably provide distributed strain measurements over long gauge fibers [21], such as those several meters in length. For instance, an optical fiber that spans 40 feet can support FBGs at one-half-inch intervals, providing ≈1,000 strain sensing points along a single fiber [22]. OFDR utilizes amplitude modulation of a continuous-wave light source, such as a laser, to obtain backscatter information in the frequency domain. Then, by using specialized fiber that contain very weak FBGs, reflections along the fiber can be enhanced to allow strain information to be inferred from the shifts in reflection [21].

This study applies the principals of OFDR to perform experimental modal analysis on a cantilevered plate. Traditional OFDR takes the frequency domain information from the FOSS and transforms it into an impulse response in the time domain through an inverse fast Fourier transform (IFFT) [21]. Applied strain causes linear shifts in the resonant wavelengths of the impulse response, which is how FOSS monitors strain [23]. However, applied strains also lead to changes in the frequency domain, which register as Doppler shifts. This study considers both the strain estimates recovered from the IFFT while also leveraging the Doppler shift data from the frequency domain, performing modal analysis on both sets of time series data. The results from the Doppler shift time histories are subsequently compared to a traditional strain-based identification. This study demonstrates that valuable modal information can be conveyed by operating directly on the original frequency domain data.

Background

The FOSS developed by NASA is based on the Langley method, using OFDR to interrogate the FBGs [23]. The sensing arm is composed of single mode fiber with continuous weak FBGs. FBGs reflect light from a particular wavelength, commonly referred to as the Bragg wavelength λ_B, while transmitting light from other wavelengths. For this system, the FBGs are written in the same wavelength, i.e., every grating has the same λ_B.

The light reflected from each weak FBG is combined with a reference signal to create an interference signal, and the resulting intensity of this interfering signal is measured by the photodetector. When received by the interrogator within the data acquisition system, the output signal represents the summation of the intensity of the interfering signal from each FBG along the fiber length, producing the type of interferogram shown in Fig. 1a. Applying a fast Fourier transform (FFT) to a chosen interferogram maps the intensity information from the wavelength domain to the spatial (frequency) domain, as shown in Fig. 1b. The resulting spatial domain information shows a series of reflections that appear as "top hats," as highlighted in Fig. 1b. These top hats are the carrier frequencies, which represent each FBG at its unique distance (position) along the sensing fiber. The resonant wavelength of each FBG is found by isolating an individual top hat and taking the IFFT from the spatial domain back to the wavelength domain.

Applied strain has a linear relationship to shifts in resonant wavelength — straining an FBG in tension or compression causes it to stretch or contract, respectively, which produces an increase or decrease in the wavelength. Thus, monitoring changes in this wavelength allows for strain to be inferred at a given FBG [23]. Assuming conventional temperature correction techniques [24], the expression relating pure mechanical strain ε to wavelength shifts is given as [25]

$$\varepsilon = \frac{1}{1-p_e}\frac{\Delta\lambda_B}{\lambda_B} \tag{1}$$

where $\Delta\lambda_B$ is the change in the resonant (Bragg) wavelength and $1/(1-p_e)$ represents a strain-optic calibration coefficient. Evaluating this expression at every sample time for a given FBG location generates its strain time history. When subjected to an applied strain the top hats also experience a shift in their carrier frequency; however, these are Doppler shifts that accumulate along the length of the fiber [26]. The difference in the position of the center of mass of each top hat, i.e., the difference in the identified carrier frequency, is proportional to the integrated strain along the length of the fiber [26].

Strain measurements, including those collected by fiber optic strain sensors, can be decomposed into a modal basis [25], as shown in Eq. (2)

$$\boldsymbol{\varepsilon}(t) = \boldsymbol{\Psi}\boldsymbol{\xi}(t) \tag{2}$$

where $\boldsymbol{\varepsilon}(t)$ is a vector containing the measured strains, $\boldsymbol{\Psi}$ is the matrix collecting normalized strain relative to the mode shape, i.e., the strain mode shape matrix, and $\boldsymbol{\xi}(t)$ is the vector of modal weights, i.e., modal coordinate vector. Equation (2)

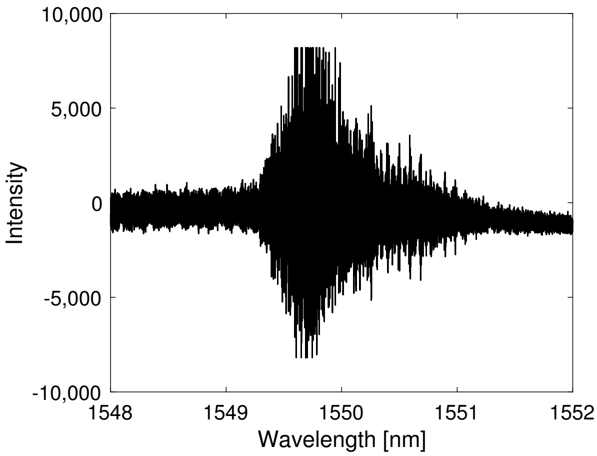

(a) Inteferogram

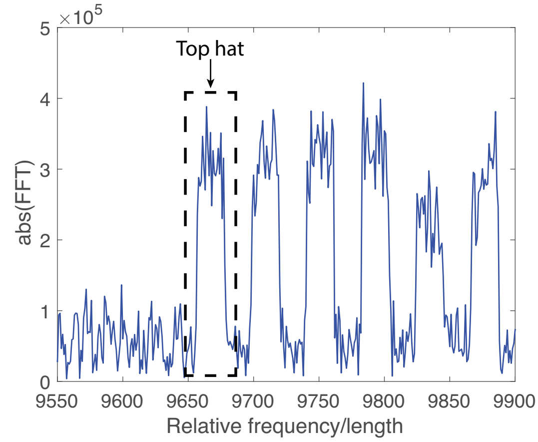

(b) FFT

Fig. 1 Original interferogram (wavelength domain) and corresponding FFT (spatial/frequency domain). Note that the FFT is shown over a windowed range for enhanced visualization.

can be utilized for modal identification, wherein modal information, such as mode shapes, are extracted from the original strain measurements. For instance, blind source separation (BSS) is a family of time domain-based techniques [27] for system identification that assumes a set of observations $\mathbf{x}$ are mixture of a set of independent sources $\mathbf{s}$, as shown in Eq. (3) with $\mathbf{A}$ denoting the "mixing" matrix.

$$\mathbf{x} = \mathbf{A}\mathbf{s}\,. \tag{3}$$

The aim of BSS is to use the observed outputs to solve for the original sources, as shown in Eq. (4)

$$\hat{\mathbf{s}} = \mathbf{W}\mathbf{x} \tag{4}$$

where $\hat{\mathbf{s}}$ is the vector of estimated source signals and $\mathbf{W}$ is the "de-mixing" matrix. It can be easily observed that Eq. (2) assumes the same form as Eq. (3), wherein the observed strains serve as the mixed signals, the modal coordinates are the independent sources, and the mode shape matrix is a mixing matrix. This study adopts the second order blind identification (SOBI) [28] to perform modal analysis and ultimately identify the strain mode shapes.

SOBI is also applied to the the time histories created by the change in carrier frequencies at a given sensing point. These carrier frequency shifts can be monitored at every sample time by tracking the change in the center of mass of each top hat, creating a time history of the Doppler shifts for a given sensing point or FBG. As mentioned previously, the shift in carrier frequency is proportional to the integrated strain, which is related to the slope of the displacement. Thus, applying the SOBI method to these time histories produces estimates of the slope mode shapes, as will be further demonstrated in the results.

Analysis

A series of tests were performed on a cantilevered test article at the NASA Neil A. Armstrong Flight Research Center. The test article is a 6061 aluminum plate 70 in. long (span) $\times$ 12 in. wide $\times$ 1/4 in. thick. The plate was cantilevered with one end bolted to a frame (clamped) while the other end remained free. The interrogating fiber for the FOSS starts 6 in. from the clamped end and includes a total of 81 FBGs along its span, as shown in the schematic illustration in Fig. 2a. A finite element (FE) model of the test article was created in FEMAP [29]. A modal analysis was performed on this model to identify the natural frequencies and mode shapes for the first four bending modes. Figure 2b shows the displacement mode shape of Mode 3 generated by the FE model. In addition to the displacement mode shapes, the strain mode shapes are also recovered from the FE model wherein profiles are extracted along the centerline of the top surface of the plate given that this is where the fiber is placed.

The test article was excited by a shaker attached to the tip of the free end that provided sinusoidal excitation at three designated frequencies. The three excitation frequencies were chosen based on the natural frequencies identified from the modal analysis of the FE model such that the test operating at 10 Hz was close to the 2nd natural frequency, 28 Hz was close to the 3rd natural frequency, and 55 Hz was close to the 4th natural frequency. Thus, each test targeted a particular

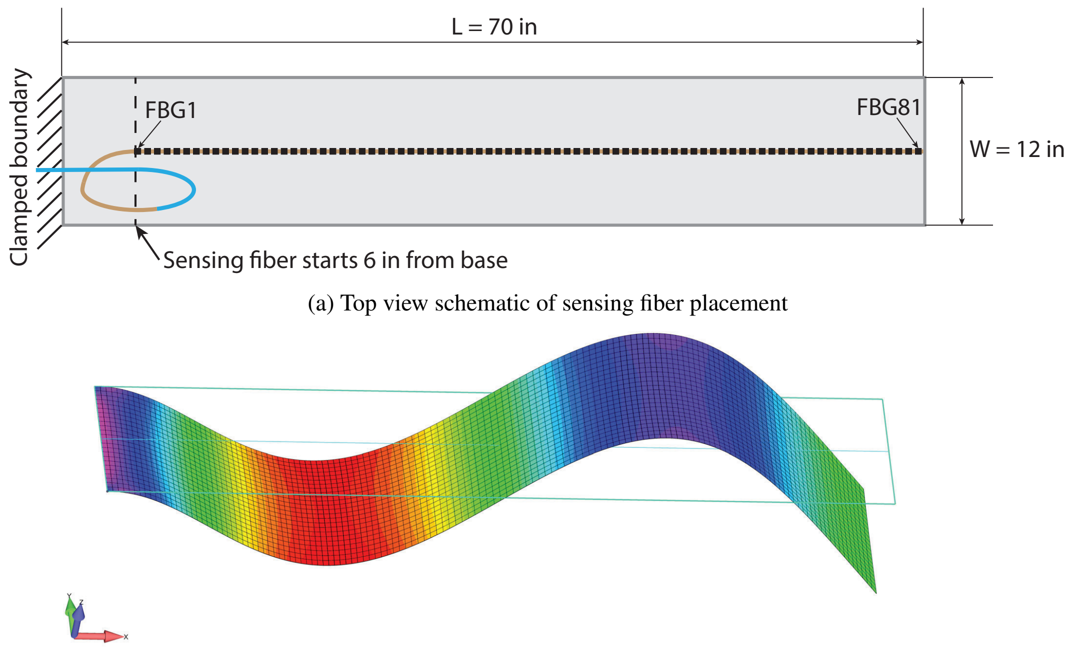

(a) Top view schematic of sensing fiber placement

(b) Displacement mode shape of Mode 3

Fig. 2 Cantilevered wing test article showing a) illustrative schematic of sensing fiber placement and b) modal analysis of finite element model.

mode. Each test lasted 15-25 s with an average test length of about 21 s. During testing, the unit had an acquisition rate of approximately 120 Hz.

When computing the strain from fiber optic measurements using Eq. (1), the change in wavelength $\Delta\lambda_B$ is always relative to some baseline. Since each test features a quiescent period of 2-4 s at its start, the baseline for each test is calculated using its first 60 measurements, which translates to the first one-half second of each recording. Once computed, all 81 strain time histories are used within the SOBI method. The first vector of the estimated mixing matrix from the 10 Hz test is plotted against the corresponding strain mode shape from the FE model in Fig. 3. Note that the strain

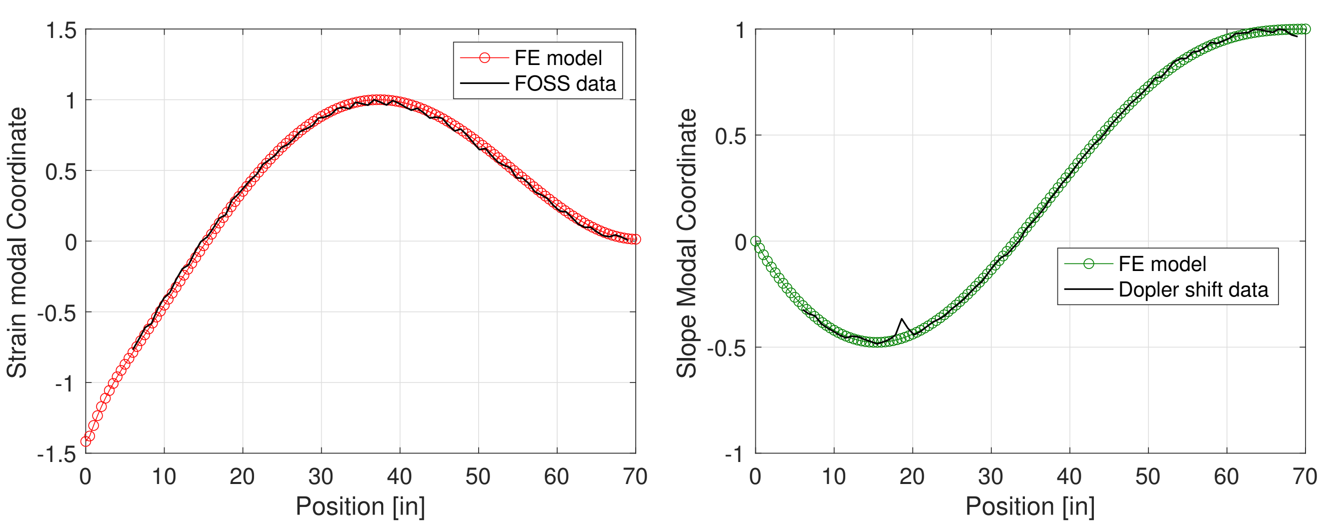

(a) Strain mode shape

(b) Slope mode shape

Fig. 3 Comparison of a) strain mode shapes and b) slope mode shapes for Mode 2 taken from the FE model and estimated from SOBI using FOSS data from 10 Hz test.

mode shapes are normalized by their maximum value, which occurs around 37 in. for both mode shapes. Also, note that estimated strain mode shape begins at 6 in. because that is the location of the first FOSS sensing point, as previously detailed.

The Doppler shift time histories are analyzed in a similar fashion as the strain time histories. One notable difference is that the Doppler shifts are relative to the initial position, meaning the baseline for the Doppler shifts is simply the initial measurement. Recall that the Doppler shift is proportional to the change in (displacement) mode shape $\boldsymbol{\phi}$ along the fiber length x, i.e., $\frac{d\boldsymbol{\phi}}{dx}$. Thus, the identified mode shape is related to the "slope" of the displacement mode shape and has to be compared to the corresponding "slope" mode shape from the FE model. The slope mode shapes in the FE model can be found by either differentiating the displacement mode shape or by integrating the strain mode shape. This study computes the FE model-based slope mode shapes through integration, and Fig. 3b compares the model-based slope mode shape against the first mode shape identified from the Doppler shift-based mixing matrix from the 10 Hz test. As can be clearly observed, the identified slope mode shape is a strong match for the model-based slope mode shape.

The similarity between mode shapes can be quantified through the modal assurance criterion (MAC) [30], which measures the correlation between mode shapes. For the purposes of this study, the MAC value is defined as

$$\mathrm{MAC}(i,j) = \frac{\left|\mathbf{A}_i^{\mathrm{T}} \boldsymbol{\psi}_j^{\mathrm{FE}}\right|^2}{\left(\mathbf{A}_i^{\mathrm{T}} \mathbf{A}_i\right)\left({\boldsymbol{\psi}_j^{\mathrm{FE}}}^{\mathrm{T}} \boldsymbol{\psi}_j^{\mathrm{FE}}\right)} \tag{5}$$

where $\boldsymbol{\psi}_j^{\mathrm{FE}}$ is the strain mode shape vector from the jth mode of the FE model and $\mathbf{A}_i$ is the ith column of the mixing matrix. The MAC value can only be computed from 6 to 70 in. due to the lack of sensing fiber along the first 6 in.; thus, the strain mode shapes are technically incomplete, which could slightly affect the computation of the associated MAC values. Note that Eq. (5) can also be used to compute the MAC values for the slope mode shapes with $\frac{d\boldsymbol{\phi}}{dx}^{\mathrm{FE}}$ serving as the reference mode shapes from the FE model.

Table 1 MAC value comparison for identified strain and slope mode shapes

Test Excitation Frequency	Strain Mode No.			Slope Mode No.		
[Hz]	2	3	4	2	3	4
10	**0.999**	**0.960**	0.359	**0.999**	**0.988**	0.782
28	0.241	**0.997**	0.206	**0.929**	**0.997**	0.723
55	0.234	0.293	**0.996**	**0.937**	0.743	**0.998**

The MAC analysis process is repeated for the strain and Doppler shift data from all three tests wherein the strain mode shapes from the FE model are compared against the identified strain mode shapes and the integrated strain mode shapes from the FE model, i.e., slope mode shapes, are compared against the identified slope mode shapes. The results are shown in Table 1. The targeted modes (diagonal entries) yield comparably high MAC values for both data sources, but the slope mode shapes have much higher MAC values for the non-targeted (off-diagonal) modes in every case. The 10 Hz test results in multiple modes with MAC values larger than 0.90 using both strain data and the Doppler shifts — MAC values greater than 0.90 are highlighted in bold — but this is the only such instance for the strain data. In contrast, the Doppler shift data yields two such MAC values for every test. This is significant because it suggests that the Doppler shift can reliably yield modal information beyond the single mode being targeted by the excitation.

Figure 4 presents two of the identified slope mode shapes for non-targeted modes. Figure 4a presents a highly compelling estimate of the slope mode shape for Mode 3 from the 10 Hz test. While the estimate for the slope mode shape for Mode 2 in Fig. 4b is much less convincing, it nonetheless correlates with the true slope mode shape, indicating that the Doppler shifts contain some modal energy from those non-targeted modes. Taken together, Table 1 and Figs. 3b and 4 demonstrate that the Doppler shift time histories contain richer modal information than strain, which suggests that dynamic signals generated from distributed FOSS systems based on OFDR possess high value modal information beyond their typical strain measurements.

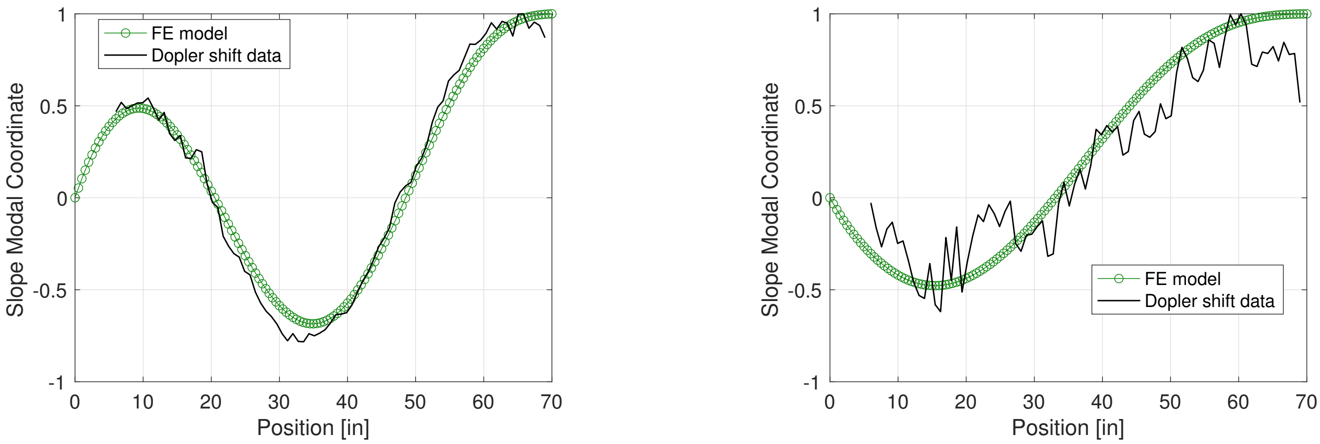

(a) Mode 3 – 10 Hz Test

(b) Mode 2 – 28 Hz Test

Fig. 4 Comparison of non-targeted slope mode shapes taken from the FE model and estimated from SOBI using FOSS data.

Conclusion

This study shows that interferograms produced from OFDR-based distributed FOSS can yield both strain time histories as well as time histories of the Doppler shifts in carrier frequencies of each weak FBG sensor along the fiber. System identification via blind source separation can then be applied to these dynamical responses to recover modal information, such as mode shapes estimates. The proposed identification approach was applied to FOSS data collected on a cantilevered plate subjected to experimental modal analysis. Using the SOBI method, strain mode shapes are recovered from strain time histories while the Doppler shift time histories yield estimates of the slope mode shapes. Using MAC values based on comparisons to reference mode shapes from an FE model, it was shown that both dynamical responses produce high quality mode shape estimates for the modes targeted by the excitation.

Crucially, this study also revealed that the Doppler shift time histories contain richer modal information than strain. This was demonstrated by the Doppler shift information producing multiple high quality mode shape estimates, i.e., MAC values greater than 0.90, for every test, while the strain time histories had only managed this once. Further, the typical MAC value produced by the slope mode shapes was noticeably larger than those from the strain data. The results of this study demonstrate that OFDR-based distributed FOSS contain multiple dynamic signals that possess high-value modal information for SHM applications, and that Doppler shift time histories should be the subject of further investigation, e.g., under operational loading conditions.

Acknowledgments The author would like to acknowledge Dr. Allen Parker, Mr. Frank Peña, and Dr. Patrick Chan at the NASA Armstrong Flight Research Center for their generosity in sharing the data from the test article as well as their several helpful discussions.

References

1. Brownjohn, J. "Structural health monitoring of civil infrastructure". *Philosophical Transactions of the Royal Society A: Mathematical, Physical and Engineering Sciences*, 365(1851):589–622 (2007).
2. Diamanti, K. and Soutis, C. "Structural health monitoring techniques for aircraft composite structures". *Progress in Aerospace Sciences*, 46(8):342 – 352 (2010).
3. Chen, S., Wang, J., Zhang, C., Li, M., Li, N., Wu, H., Liu, Y., Peng, W., and Song, Y. "Marine structural health monitoring with optical fiber sensors: A review". *Sensors*, 23(4) (2023).
4. Worden, K., Farrar, C.R., Haywood, J., and Todd, M. "A review of nonlinear dynamics applications to structural health monitoring". *Structural Control and Health Monitoring*, 15(4):540–567 (2008).
5. Glisic, B. and Inaudi, D. *Fibre optic methods for structural health monitoring*. John Wiley & Sons (2008).
6. Dalla Vedova, M.D.L., Berri, P.C., Maggiore, P., and Quattrocchi, G. "Design and development of innovative FBG-based fiber optic sensors for aerospace applications". *Journal of Physics: Conference Series*, 1589(1):012012 (2020).
7. Min, R., Liu, Z., Pereira, L., Yang, C., Sui, Q., and Marques, C. "Optical fiber sensing for marine environment and marine structural health monitoring: A review". *Optics & Laser Technology*, 140:107082 (2021).

8. Udd, E. “An overview of fiber-optic sensors”. *Review of Scientific Instruments*, 66(8):4015–4030 (1995).
9. Murayama, H., Kageyama, K., Naruse, H., Shimada, A., and Uzawa, K. “Application of fiber-optic distributed sensors to health monitoring for full-scale composite structures”. *Journal of Intelligent Material Systems and Structures*, 14(1):3–13 (2003).
10. Cazzulani, G., Silva, A., and Pennacchi, P. “Optimization of continuous sensor placement for modal analysis: Application to an optical backscatter reflectometry strain sensor”. *Mechanical Systems and Signal Processing*, 150:107242 (2021).
11. Brownjohn, J.M.W., De Stefano, A., Xu, Y.L., Wenzel, H., and Aktan, A.E. “Vibration-based monitoring of civil infrastructure: challenges and successes”. *Journal of Civil Structural Health Monitoring*, 1(3):79–95 (2011).
12. Anastasopoulos, D., De Smedt, M., Vandewalle, L., De Roeck, G., and Reynders, E.P.B. “Damage identification using modal strains identified from operational fiber-optic Bragg grating data”. *Structural Health Monitoring*, 17(6):1441–1459 (2017).
13. Jiang, X., Li, B., Mao, X., Peng, Y., and He, S. “New approach based on operational strain modal analysis to identify dynamical properties of the high-speed reciprocating operation mechanism”. *Journal of Low Frequency Noise, Vibration and Active Control*, 38(3-4):1345–1362 (2019).
14. Wang, T., Celik, O., Catbas, F., and Zhang, L. “A frequency and spatial domain decomposition method for operational strain modal analysis and its application”. *Engineering Structures*, 114:104–112 (2016).
15. Reynders, E., De Roeck, G., Gundes Bakir, P., and Sauvage, C. “Damage identification on the Tilff bridge by vibration monitoring using optical fiber strain sensors”. *Journal of Engineering Mechanics*, 133(2):185–193 (2007).
16. Anastasopoulos, D., Moretti, P., Geernaert, T., De Pauw, B., Nawrot, U., De Roeck, G., Berghmans, F., and Reynders, E. “Identification of modal strains using sub-microstrain FBG data and a novel wavelength-shift detection algorithm”. *Mechanical Systems and Signal Processing*, 86:58–74 (2017).
17. Wang, Z., Liu, M., Qu, Y., Wei, Q., Zhou, Z., Tan, Y., Hong, L., and Song, H. “The detection of the pipe crack utilizing the operational modal strain identified from fiber Bragg grating”. *Sensors*, 19(11) (2019).
18. Anastasopoulos, D., Maes, K., De Roeck, G., Lombaert, G., and Reynders, E.P.B. “Influence of frost and local stiffness variations on the strain mode shapes of a steel arch bridge”. *Engineering Structures*, 273:115097 (2022).
19. Murayama, H., Igawa, H., Omichi, K., and Machijima, Y. “Distributed sensing with OFDR and its application to structural health monitoring”. *Proceedings of SPIE - The International Society for Optical Engineering*, 7753 (2011).
20. Liang, C., Bai, Q., Yan, M., Wang, Y., Zhang, H., and Jin, B. “A comprehensive study of optical frequency domain reflectometry”. *IEEE Access*, 9:41647–41668 (2021).
21. Liehr, S., Nöther, N., and Krebber, K. “Incoherent optical frequency domain reflectometry and distributed strain detection in polymer optical fibers”. *Measurement Science and Technology*, 21(1):017001 (2009).
22. Peña, F. “Fiber-optic strain-based deflection and twist sensing for a high-aspect-ratio swept wing”. Technical Report TM-2020-220465, NASA (2020).
23. Richards, W.L., Parker Jr, A.R., Ko, W.L., Piazza, A., and Chan, P. “Application of fiber optic instrumentation”. RTO-AG-160, Vol. 22, SCI-228, NATO Research and Technology Organization (RTO) (2012).
24. Dally, J.W. and Riley, W.F. *Experimental Stress Analysis*. McGraw-Hill, New York, 3rd edition (1991).
25. Kang, L.H., Kim, D.K., and Han, J.H. “Estimation of dynamic structural displacements using fiber Bragg grating strain sensors”. *Journal of Sound and Vibration*, 305(3):534–542 (2007).
26. Peña, F., Park, B.C., and Chin, A. “Examination of doppler fiber optic sensing for structural velocity estimations”. Technical Report TM-20210025579, NASA (2021).
27. Jutten, C. and Herault, J. “Blind separation of sources, part I: An adaptive algorithm based on neuromimetic architecture”. *Signal processing*, 24(1):1–10 (1991).
28. Belouchrani, A., Abed-Meraim, K., Cardoso, J.F., and Moulines, E. “A blind source separation technique using second-order statistics”. *IEEE Transactions on signal processing*, 45(2):434–444 (1997).
29. Siemens PLM. *FEMAP User Guide* (2020).
30. Allemang, R.J. “A correlation coefficient for modal vector analysis”. In *Proceedings of the 1st International Modal Analysis Conference (IMAC)*, pages 110–116 (1982).